PCCP

PAPER

Check for updates

Photophysics and photochemistry of carminic acid and related natural pigments†

Margherita Zucchelli,‡[abf] Fernando D. Villarruel,‡[ac] Pedro David-Gara,[d] Mariana R. Costante,[c] Marcos Tascon,[be] Fernando Marte,*[b] Fernando S. García Einschlag*[c] and Franco M. Cabrerizo [ID] *[a]

Carminic acid (CA) and other related compounds have been widely used as dyes in cultural heritage, cosmetics and the food industry. Therefore, the study of their properties upon photoexcitation is particularly important. In this work, the photophysical and photochemical properties of CA, carminic lake and other related pigments in aqueous solutions are revisited. Novel quantitative information regarding the fate of the photoexcited states is provided including the efficiency of reactive oxygen species (ROS) photosensitized production (*i.e.*, singlet oxygen and hydrogen peroxide) as well as the efficiency of nonradiative deactivation pathways. Laser-induced optoacoustic spectroscopy (LIOAS) data revealed that for all the investigated compounds, almost all the absorbed energy is released as prompt heat to the media. This is in agreement with the fact that other deactivation pathways, including fluorescence ($\Phi_F \sim 10^{-3}$–10^{-5}), photochemical degradation ($\Phi_R \sim 10^{-4}$) and/or photosensitized ROS formation ($\Phi_{H_2O_2} < 10^{-5}$ and $\Phi_\Delta \sim 0$), are negligible or null. In addition, a comprehensive investigation of the photo-degradation of CA and lake is herein reported. The influence of different experimental parameters such as irradiation wavelength and oxygen partial pressure was evaluated. UV-vis absorption and fluorescence emission spectroscopy in combination with chemometric data analysis were used to elucidate the relevant aspects of the photodegradation mechanism involved and the spectroscopic features of the photoproducts generated. In aqueous media, CA follows an O_2-dependent photochemical degradation when subject to elapsed photoexcitation in the UVB, UVA and visible regions. The photoproduct profile depends on the excitation wavelength giving rise to quite distinctive spectroscopic profiles. With respect to lake, our data suggest that upon photoexcitation, this pigment releases a CA-like chromophore that follows a similar fate to CA.

1. Introduction

Carminic acid (CA) is a red dye that consists of hydroxyanthraquinones linked to a glucose unit. This compound is originally obtained from Central America, specifically extracted from the dried bodies of the female scale insect Coccus cacti (*Dactylopius coccus Costa*).[1,2] The first reported usages in art,

as a colorant called cochineal, were from Aztec,[1] Inca[3] and Hispanic colonial cultures[4,5] and it was mainly used in textiles and paintings. Later, after the conquest of America in the 16th century, the material was exported to Europe where it was widely utilized in paintings.[1] Indeed, it has been found in European art works from the 16th century[6] to the early-20th century.[7,8] Due to its fugitive nature, CA is also used in

[a] Instituto Tecnológico de Chascomús (INTECH), Universidad Nacional de San Martín (UNSAM) – Consejo Nacional de Investigaciones Científicas y Técnicas (CONICET), Av. Intendente Marino Km 8.2, CC 164 (B7130IWA), Chascomús, Argentina. E-mail: fcabrerizo@intech.gov.ar

[b] IIPC-Tarea, Universidad Nacional de San Martin, Quinquela Martin 1784, CABA, Argentina. E-mail: fmarte.iipc@gmail.com

[c] INIFTA – CONICET, Universidad Nacional de La Plata, Diag. 113 y 64 (1900), La Plata, Argentina. E-mail: fgarciae@quimica.unlp.edu.ar

[d] Centro de Investigaciones Ópticas (CIOp; CONICET – CIC – UNLP), C.C. 3 (1897) Gonnet, Bs. As., Argentina and Dpto. de Química, Fac. de Ciencias Exactas, Universidad Nacional de La Plata, Argentina

[e] Instituto de Investigación e Ingeniería Ambiental (IIIA), Universidad Nacional de San Martín (UNSAM) – Consejo Nacional de Investigaciones Científicas y Técnicas (CONICET), San Martin, Buenos Aires, Argentina

[f] Dipartimento di Scienze Ambientali, Informatiche e Statistiche, Campus Scientifico, Università Ca' Foscari di Venezia, Via Torino 155 (30170), Venezia Mestre, Italia

student-grade artists' paints.[2,9] In addition, CA and other relevant pigments represent a set of colorants widely used in cosmetics and the food industry. Thus, the study of the physicochemical properties of these molecules is highly relevant.[10–12] In the particular case of CA, the degradation properties can be evaluated by investigating the free pigment and/or the corresponding lake. The latter is composed by a metal, typically aluminium, complexed with two CA molecules at their central carbonyl and adjacent hydroxyl positions. Regarding thermal stability, the lake was demonstrated to be highly resistant to high temperatures in the presence of oxygen.[2,13] On the other hand, previous studies dealing with the photodegradation of CA pointed out the changing of lake colour with aging. In this manner, pioneering studies at the beginning of the 2000's investigated the role of protolytic interactions in the photodegradation of CA and their lakes.[14] Essentially, spectral differences were found between irradiated and nonirradiated samples. Most of the photoproducts were absorbed in the UVA region, resulting in colour fading rather than a change in colour. The CA mixed with arabic gum (binder) was less photo-stable than the corresponding aqueous solution, and the aluminium lake presented better stability. Furthermore, it was demonstrated that in anoxic environments, the aluminium lake degradation rate decreases drastically. The binder plays a role in pigment degradation under anoxic conditions, with the greatest colour stability observed for the oil colour, followed by the water colour and pure dye on paper.[15–18] In addition, Bowers and Sobeck have reported[19] a comprehensive study on the photoaging of CA and its lake as a function of different experimental parameters such as oxygen content, humidity and binder. However, several aspects of the mechanisms of CA photodegradation still need to be addressed. Moreover, a thorough characterization of the photoproducts that trigger or accelerate the degradation of CA would certainly have several ramifications in the field of art restoration and conservation.

Against this background, new insights into the photodegradation process of CA, carminic lake and other related compounds (Scheme 1) in aqueous media are herein reported. Following this line, the quantum yields of singlet oxygen ($^1O_2$) and hydrogen peroxide (H_2O_2) production were quantified. By using laser induced optoacoustic spectroscopy (LIOAS), nonradiative deactivation pathways were characterized for the first time. Besides, the photodegradation of CA and lake excited with UVB and UVA radiation in aqueous media is described. The effects of different experimental parameters on the photodegradation mechanism were also investigated. Parallel Factor Analysis (PARAFAC) was applied to further elucidate the formation of photoproducts as well as both their kinetic profiles and main spectral features. Finally, the mechanisms of photodegradation for both CA and lake are presented.

2. Experimental

2.1. Materials and supplies

Carminic acid (CA), Alizarin (ALI), New Coccine (NC), sodium azide and superoxide dismutase (SOD) from bovine erythrocytes
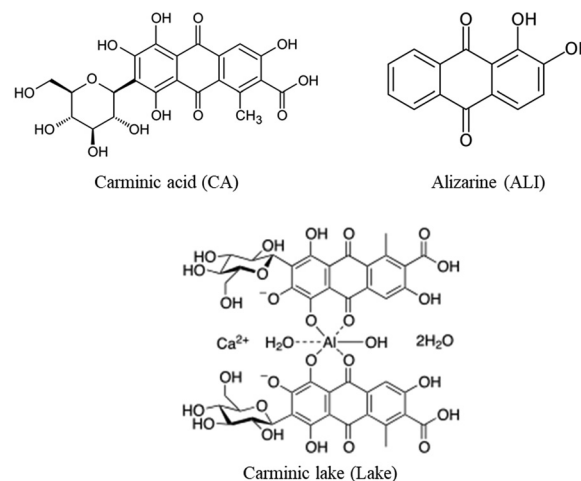
Scheme 1 Molecular structure of the compounds investigated in this work.

were provided by Sigma-Aldrich whereas the aluminium–calcium complex of carminic acid (referred as carmine, carminic lake or, simply, lake) was provided by *Colores Naturales de Oaxaca* (Oaxaca, Mexico). Ultrapure water was obtained from a Milli Q water purification system (Millipore, USA) while hydrochloric acid (HCl) and sodium hydroxide were acquired from Merck. All the chemicals and reagents were purchased at the highest purity available and used without further purification. Research grade (5.0) N_2 gas was used to decrease the oxygen partial pressure in the samples.

2.2. Determination of singlet oxygen ($^1O_2$) production

The efficiency of colorants towards singlet oxygen sensitization was assessed by the direct measurement of the $^1O_2$ ($^1\Delta_g$) near-IR phosphorescence at 1270 nm. Time-resolved phosphorescence of $^1O_2$ ($^1\Delta_g$) was observed at 90° geometry by means of a pre-amplified (low impedance) Ge-photodiode (Applied Detector Corporation, time resolution 1 µs). A simple exponential analysis of the emission decay was performed. The quantum yield of $^1O_2$ ($^1\Delta_g$) formation, Φ_Δ, was determined by measuring its phosphorescence intensity using optically matched solutions of phenalenone (Phen) ($\Phi_\Delta = 0.98$)[20] and Rose Bengal ($\Phi_\Delta = 0.75$)[21] as reference sensitizers for ACN and D_2O solutions, respectively.

2.3. Laser Induced Optoacoustic Spectroscopy (LIOAS) experiments

Photoacoustic measurements were performed using the setup described elsewhere.[22] Briefly, a Q-switched Nd:YAG laser (Surelite II, continuum, 7 ns pulse duration, 532 nm, UK) was used as the excitation source. The fluence of the laser pulses was varied using a neutral density filter, and the energy values were measured with pyroelectric energy meters (Laser Precision Corp. RJ7620 and RJP-735). The laser beam was shaped by a 1 mm diameter pinhole in front of the cuvette, so that the resolution time in our experimental set-up, t_R, was *ca.* 800 ns.[23] The detection system consisted of a 4 mm thick × 4 mm in a diameter home-made ceramic piezoelectric transducer (PZT),

This journal is © the Owner Societies 2020

Phys. Chem. Chem. Phys., 2020, **22**, 9534–9542 | **9535**

pressed against a cuvette side wall parallel to the laser beam direction. The detected acoustic signals were amplified, digitized by a digital oscilloscope (TDS 3032, Tektronix), and stored in a personal computer for further analysis of data. Measurements were performed by averaging the acoustic signals generated by 64 laser shots for a better signal-to-noise ratio. Aqueous solutions of the samples and a calorimetric reference (CR, New Coccine, $\alpha_R = 1$) were matched within 2% of absorbance values between 0.1 and 0.2 at the laser wavelength.[24] Experiments were performed under a controlled atmosphere, obtained by purging the solutions with N_2 or O_2, for 15 min.

2.4. Steady irradiation

Aqueous solutions of CA at pH 4.2 (where CA is present at more than 99% in the mono-anionic form)[25] were irradiated using the irradiation set-up described elsewhere.[26–28] Briefly, CA solutions were irradiated at different irradiation wavelengths in 1 cm quartz cells under a controlled temperature (20.0 ± 0.1 °C). Four different 8 Watt lamps were used as excitation sources: (i) three Rayonet RPR (Southern N.E. Ultraviolet Co.) lamps, with emission spectra centred at 300, 350 and 420 nm (a fwhm bandwidth of ~15 nm) and (ii) a Phillips lamp with an emission spectrum at 365 nm (a fwhm bandwidth of ~20 nm). For comparison purposes, the absorbance of the solutions, at the excitation wavelength, was matched at 0.40. Absorption spectra of the solutions were recorded at regular intervals of irradiation time. Difference spectra were obtained by subtracting the spectrum at time $t = 0$ from the subsequent spectra recorded at different irradiation times. Each difference spectrum was normalized relative to the maximum absolute value of the absorbance difference, yielding the normalized difference (ND) spectrum.[29] The role of dissolved molecular oxygen and/or different reactive oxygen species (ROS) in the mechanism of the photochemical reactions was further investigated by performing experiments under different oxygen partial pressures (i.e., in air-equilibrated and N_2-saturated aqueous solutions) and/or in the presence of selective ROS scavengers (i.e., sodium azide and SOD, in order to evaluate the role of singlet oxygen ($^1O_2$) and superoxide anion ($O_2^{\bullet-}$), respectively). Deoxygenated solutions were obtained by purging with N_2 gas for 20 min.[26–28] Due to the very low solubility of lake in water, the latter pigment was firstly dissolved in DMSO and was then diluted in water (the final DMSO concentration was kept below 1%). Lake solutions were irradiated under the same conditions as described above.

2.5. UV-vis spectroscopy

UV-visible spectra were obtained using a Lambda 25 spectrophotometer (PerkinElmer). Each spectrum was acquired in the range between 200 and 700 nm with a resolution of 1 nm. A quartz cell with an optical pathway of 1 cm was utilized for the experiments.[28,30] The final concentrations of the CA and lake solutions were calculated according to the Beer–Lambert's equation using the corresponding molar absorption coefficients (ε) reported in the literature:[31] ε^{468nm} of 2.6×10^3 M^{-1} cm^{-1} and ε^{518nm} of 5.8×10^3 M^{-1} cm^{-1} for CA and lake, respectively.

2.6. Fluorescence spectroscopy

Excitation-Emission Matrices (EEMs) were recorded using a Fluoromax4 spectrofluorometer (HORIBA Jobin Yvon).[30] The instrument consists of a xenon lamp, two monochromators (for excitation and emission, respectively) and an R928 photomultiplier. The data were processed using a PC with the FluorEssence™ software. Matrices were acquired using scanning emission spectra (in the range between 250 and 600 nm with a resolution step of 2 nm) under consecutive and progressive excitation wavelengths (ranging from 296 and 700 nm, with a resolution of 5 nm). Corrected EEMs were obtained by taking into account the emission spectrum of the excitation lamp as well as the response (sensitivity) of the photomultiplier (detector).

2.7. Chemometric analysis

PARAFAC algorithm described elsewhere[30] was used to estimate the relative concentration and spectral profiles of the species formed during the photochemical reactions.

3. Results and discussion

3.1. Photophysics of CA, lake and related pigments

The extremely low quantum yields of fluorescence ($\Phi_F \sim 10^{-3}$–10^{-5}) and photochemical degradation ($\Phi_R \sim 10^{-4}$) of CA and other related pigments have been well documented.[14,32–34] Hence, these two processes do not represent the major deactivation pathways of the photoexcited dyes. To date, the main deactivation pathways as well as the mechanisms involved in the photochemical degradation of these dyes still need to be addressed.

To begin with, the quantum yield (Φ_Δ) of singlet oxygen ($^1O_2$) production by the dyes was measured with two different solvents (i.e., D_2O and acetonitrile solutions). Time-resolved phosphorescence signals (Fig. 1a) show that $^1O_2$ is either not produced or its concentration is below the detection limit. Moreover, the latter result also suggests that triplet formation is not the major route in the overall deactivation of the singlet electronic excited state of CA and the related pigments.

In order to investigate other deactivation pathways such as non-radiative decays, LIOAS experiments were performed. Results show that all the investigated dyes presented photoacoustic signals similar to the ones obtained for CR (Fig. 1b). As discussed previously by several authors,[23,35] prompt heat refers to the heat generated by the transducer in processes occurring in a time faster than roughly $\tau_R/5$, where τ_R is the transit acoustic time of the experiment. In the case of CR, all the deactivation processes take place in a time shorter than $\tau_R/5$. Then, when deactivation of the sample occurs in a time $t < \tau_R/5$, no temporal shift between the sample and the reference could be expected, and the peak-to-peak amplitude of the first acoustic pulse (H) was used to measure the prompt heat released to the medium by the sample after excitation (amplitude method).[20] In all the cases, plots of H as a function of the excitation fluence (F) measured under three different
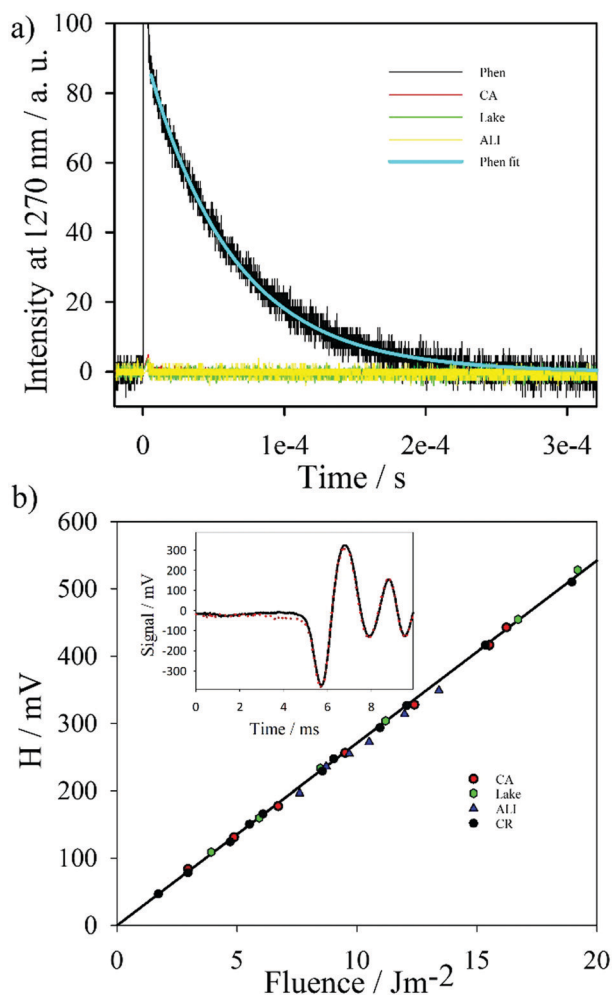
a)

b)

Fig. 1 (a) $^1O_2$ ($^1\Delta_g$) phosphorescence rise and decay signals for the reference (Phen) and the dyes in ACN solution. In cyan is the exponential decay fitting of the Phen signal (b) amplitude of the photoacoustic signals as a function of laser fluence for aqueous solutions of the four dyes and the calorimetric reference (CR) with matched absorbances (A^{532nm} = 0.12 ± 0.02). Inset: Normalized photoacoustic representative signals of aqueous solutions for CR (solid black line) and CA dye (red dotted line).

oxygen partial pressures (N_2-saturated, air-equilibrated and O_2-saturated solutions) showed a linear relationship. Slopes observed

for all the investigated dyes and the calorimetric reference CR ($\alpha_R = 1$) were the same (Fig. 1b). Data showed good reproducibility at different absorbances for fluences lower than 22 J m^{-2} (data not shown). These results can be interpreted by using the following equation:[23]

$$H/F = K\alpha(1 - 10^{-A}) \qquad (1)$$

where K is an experimental constant of the thermoelastic properties of the solution and instrumental factors, A is the absorbance of the sample at the excitation wavelength (532 nm), and α is the fraction of energy released to the medium as prompt heat. Thus, when comparing the ratio of H/F (slopes) values obtained for the sample and reference (both have the same absorbance at the excitation wavelength), α of 1.00 ± 0.05 is obtained for all the cases. This means that these dyes release to the medium the absorbed energy mostly as prompt heat. No evidence was found for the formation of photoproducts or intermediate species with lifetimes longer than this time (*i.e.*, triplet state; photo-tautomer). Therefore, for these compounds, independent of the atmosphere used, it can be assumed that the lifetimes of the triplet states are shorter than 200 ns.

3.2. Photochemistry of CA

Although having a very low quantum efficiency ($\Phi_R \sim 10^{-4}$),[31,32] the photochemical changes on CA can be observed when subject to continuous and cumulative irradiation. Since the chemical nature of the photoproducts formed as well as the photochemical processes and the mechanisms involved still remain unclear, the photodegradation reaction of CA in aqueous solution was studied. The effects of different experimental parameters such as the energy of the excitation light and the oxygen partial pressure were evaluated.

Irradiation of air-equilibrated aqueous solutions of CA (pH 4.2) was monitored using UV-vis absorption spectroscopy (Fig. 2 and Fig. S1, ESI†). Both the extent of the photodegradation reaction and the spectroscopic profile depend on the excitation wavelength used. The highest changes were observed when the solution was irradiated with 300 nm (Fig. 2b). Moreover, the photodegradation profile induced by the latter lamp differs from those induced by the other three excitation wavelengths used. This is better shown by the normalized
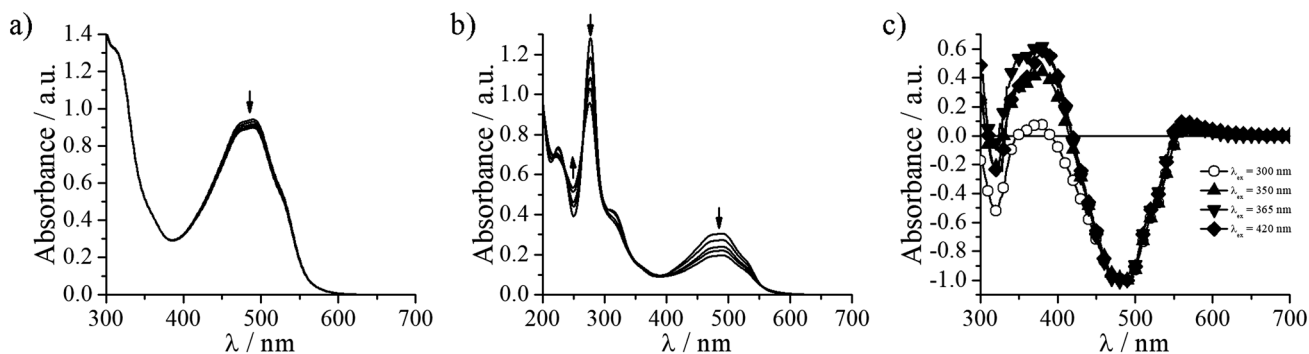
a)

b)

c)

Fig. 2 Evolution of the absorbance UV-vis spectra of CA using different excitation wavelengths ($h\nu$): (a) 420 nm and (b) 300 nm. (c) Normalized difference (ND) spectra were obtained from the UV-vis absorption spectra recorded at 6 h and the initial spectrum (t = 0 h).

This journal is © the Owner Societies 2020

Phys. Chem. Chem. Phys., 2020, **22**, 9534–9542 | **9537**

difference spectra (Fig. 2c) where the major changes are observed in the spectral domain ranging from 310 nm to 410 nm (see discussion below).

To further characterize the spectroscopic pattern of the photoproduct formed, a new set of experiments were run using, as representative examples, 300 nm and 420 nm lamps as the excitation sources. Larger irradiation times were used in order to increase the total photochemical conversion of CA. UV-visible absorption and fluorescence spectra were analysed. Inspection of the new EEM datasets showed that as long as the photochemical reaction progresses, the emission band of CA (centred at 590 nm) clearly decreases (Fig. 3 and Fig. S2, S3, ESI†). The photodegradation of CA is markedly faster when using a lamp with $h\nu = 300$ nm. This is observed from the substantial decrease of both the UV-vis absorption and emission intensities ascribed to CA. In addition, CA photodegradation gives rise to the formation of new emission spots in the range of 420–480 nm of the EEMs. It is also noted that, at longer irradiation times, a shift or distortion in the shape of the latter spot is observed. This fact suggests that secondary photodegradation processes might be taking place when subject to $h\nu = 300$ nm (see below).

Parallel factor analysis (PARAFAC) was used to decompose the three-way data arrays obtained by stacking the EEMs recorded under irradiation conditions. Briefly, four major contributions were required to reproduce the entire dataset. The resolved excitation and emission loadings are depicted in Fig. 4a, whereas the score profiles representing the contributions of each species under different conditions are compared in Fig. 4b. The excitation and emission spectra obtained for Factor #1 (*i.e.*, F #1, with bands centred at Ex/Em: 485/595 nm) fully match with that corresponding to CA. Three additional
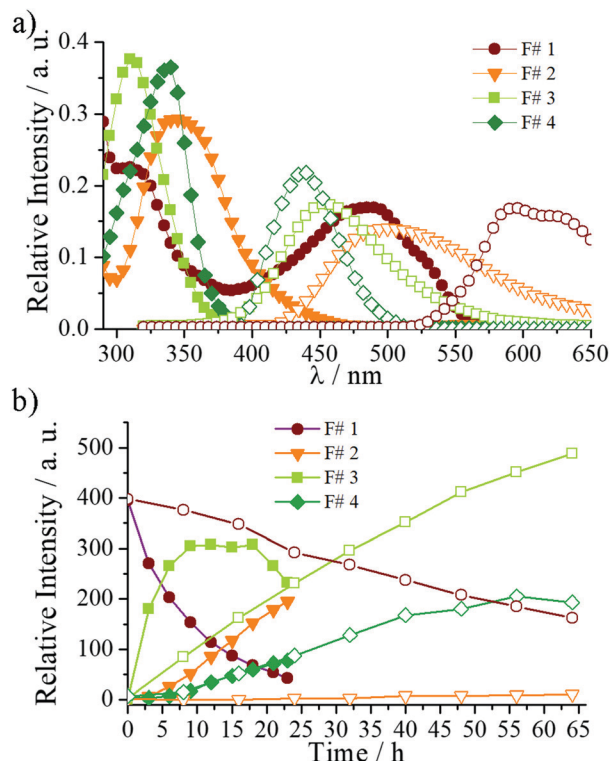

Fig. 4 (a) Normalized excitation (filled symbols) and emission (empty symbols) spectra of CA and the products generated upon irradiation obtained by a PARAFAC algorithm applied to the full tensor built from fluorescence excitation–emission matrices (EMMs) recorded in the air-equilibrated aqueous solution upon photoexcitation at the four wavelengths investigated. (b) Comparison of the relative concentration profiles obtained from PARAFAC analysis for CA and the three products detected upon photoexcitation at $h\nu = 300$ nm (filled symbols) and 420 nm (empty symbols).
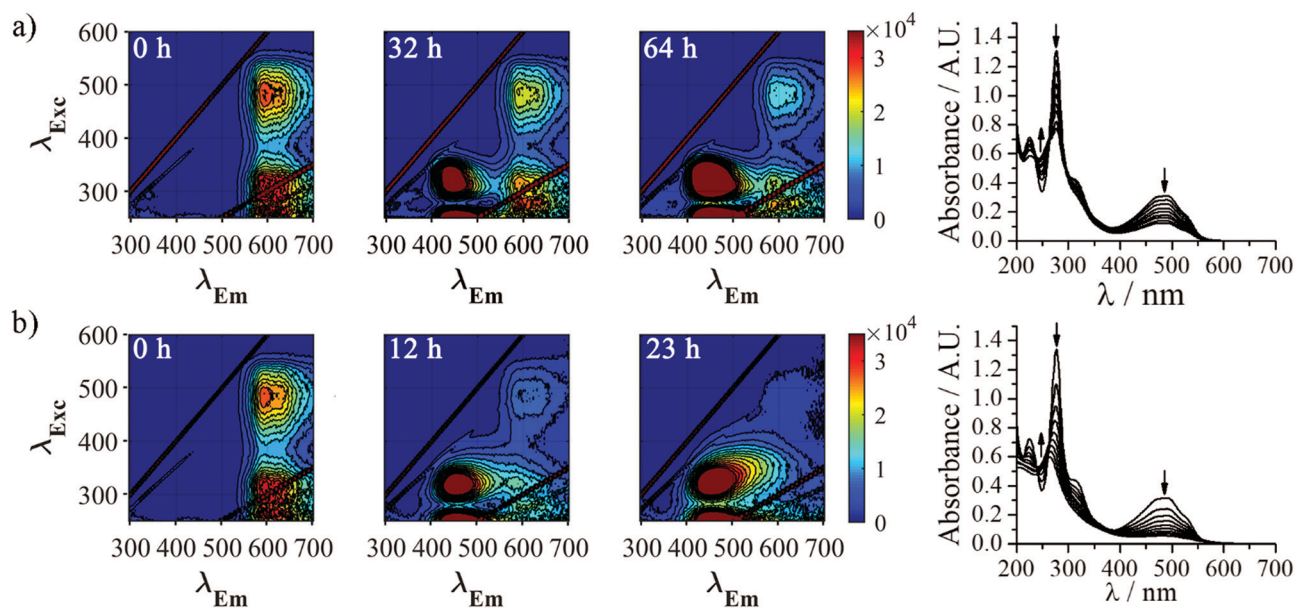

Fig. 3 Evolution of the EEMs (left panel) and UV-vis absorption spectra (right panel) of CA ([CA]$_0$ = 110 μM) irradiated aqueous solution: (a) $h\nu = 420$ nm (total irradiation time = 64 h) and (b) $h\nu = 300$ nm (total irradiation time = 23 h).

9538 | *Phys. Chem. Chem. Phys.*, 2020, **22**, 9534–9542

This journal is © the Owner Societies 2020

factors (*i.e.*, F #2, F #3 and F #4, with bands centred at Ex/Em: 345/500, 310/452 and 340/440 nm, respectively) were necessary in order to completely reproduce the entire set of EEM recorded during the irradiation experiments with different lamps. Analysis of Fig. 4b reveals that CA decays much faster upon irradiation at 300 nm than under irradiation at 420 nm. In addition, the timescales associated with Factor #3 production match with those of CA decay indicating that F #3 is the primary product. In contrast, a significant production of F #2 is observed only under irradiation at 300 nm and the kinetic profiles of both F #2 and F #3 together with the spectral features of F #3 suggest that F #2 formation is triggered by the irradiation of F #3.

Finally, the kinetic profiles obtained for Factor F #4 are much less dependent on the irradiation wavelength. In order to gain further insight into the nature of the process that leads to the formation of F #4, additional tests were performed. The CA solutions were irradiated for 20 h using the 420 nm lamp and then kept in the dark for up to 50 h. The recorded EEM showed that, upon storage under dark conditions, a fluorescence spot appeared in the Ex/Em domain of 340/440 nm. Since non-irradiated CA solutions were stable for more than 96 h, the latter result suggested that F #4 is formed from the primary photoproduct (F #3) through a non-photochemical pathway.

The role of molecular oxygen and ROS in the mechanism of CA photodegradation was also investigated. To begin with, under comparative experimental conditions, air-equilibrated and N_2-saturated aqueous solutions of CA (340 μM) were irradiated at 420 nm. Contrary to what has been reported by Kunkely *et al.*,[31] the kinetics of the overall photochemical process depend on the oxygen partial pressure. Both UV-vis absorption spectra and EEM evolution show an extremely small CA degradation ($<$7% after 6 h) in N_2-saturated solutions (Fig. 5). Given that the difference absorption spectra obtained under both atmospheric conditions show the same shape (Fig. S4a, ESI†), the former reaction may be attributed to the very small contribution of the O_2 traces remaining in the solution. Hence, it may be assumed that this reaction is O_2-dependent.

Along with photo-triggered degradation of an organic compound, molecular O_2 might play a role through different mechanisms. For example, in many cases, *in situ* photosensitized singlet oxygen $^1O^2$ (from triplet molecular O_2) may strongly react with organic molecules giving rise to its concomitant photo-oxidation. However, this might not be the case for the reaction under study since CA does not produce $^1O_2$ in a quantitative way (Fig. 1a). This hypothesis was confirmed by experiments performed in the presence of sodium azide, where no differences were observed with respect to CA solutions irradiated in the absence of this $^1O_2$-scavenger (Fig. S7, ESI†).

On the other hand, among other processes, O_2 can be involved in electron transfer reactions with the photoexcited dye giving rise to the formation of a superoxide anion ($O_2^{\bullet-}$) and an oxidized organic dye.[26,27,36,37] The photosensitized formation of $O_2^{\bullet-}$ was previously suggested by Stapelfeldt *et al.*[25] To further investigate this hypothesis, the production of H_2O_2 from irradiated CA air-equilibrated solutions was monitored herein. Note that the spontaneous disproportionation of $O_2^{\bullet-}$ can give rise to the formation of H_2O_2 in a pH-dependent reaction showing the highest rate values at pH $\sim$ 4.8 (*i.e.*, the pK_a of the acid base equilibrium between $O_2^{\bullet-}$ and its conjugate acid $HO_2^{\bullet}$). Therefore, CA samples were irradiated under the same experimental conditions as those used for the determination of CA bleaching (see above). Data reflect that, although with low efficiency, photoinduced formation of H_2O_2 was detected (Fig. S5, ESI†). Moreover, the amount of H_2O_2 correlates well with the amount of CA consumed. Therefore, the production of H_2O_2, as a result of $O_2^{\bullet-}$ disproportionation may be a source of H_2O_2 that is applicable in this work.

To further evaluate the role of $O_2^{\bullet-}$ in the main mechanism of CA photodegradation, air-equilibrated CA solutions were irradiated (420 nm) in the presence of superoxide dismutase, SOD (Fig. S6, ESI†). Data show that the overall process has the same trend as that presented for CA air-equilibrated solutions irradiated in the absence of SOD. Hence, it can be inferred that despite the fact that the reaction process is driven by O_2, and albeit that a superoxide anion might be present in the solution, the role of ROS in the overall CA photodegradation may be considered to be negligible or null.

3.3. Photochemistry of aluminium lake

In the lake, some specific photophysical properties (*i.e.*, yield of singlet oxygen production and the efficiency of the non-radiative deactivation pathways) remain the same as CA (see above),
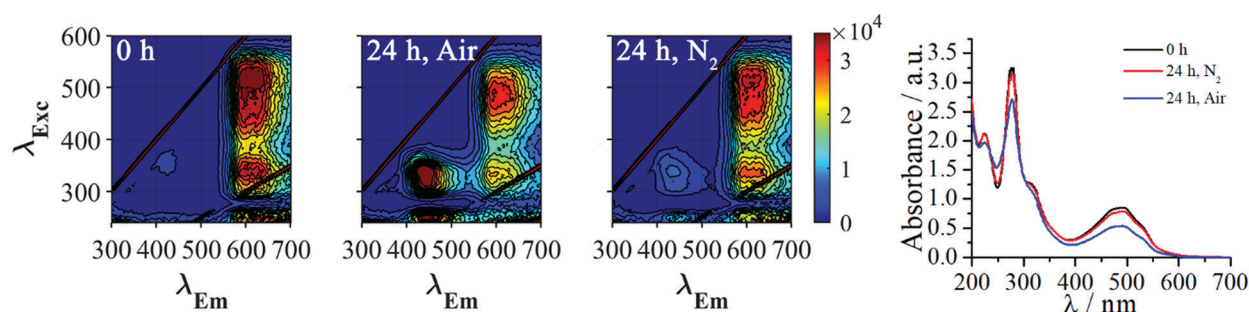

Fig. 5 Evolution of the EEMs (left panel) and UV-vis absorption spectra (right panel) of CA ([CA]$_0$ = 340 μM) irradiated aqueous solution ($h\nu$ = 420 nm; total irradiation time = 24 h) under different oxygen partial pressures for air-equilibrated and N_2-saturated solutions.

This journal is © the Owner Societies 2020

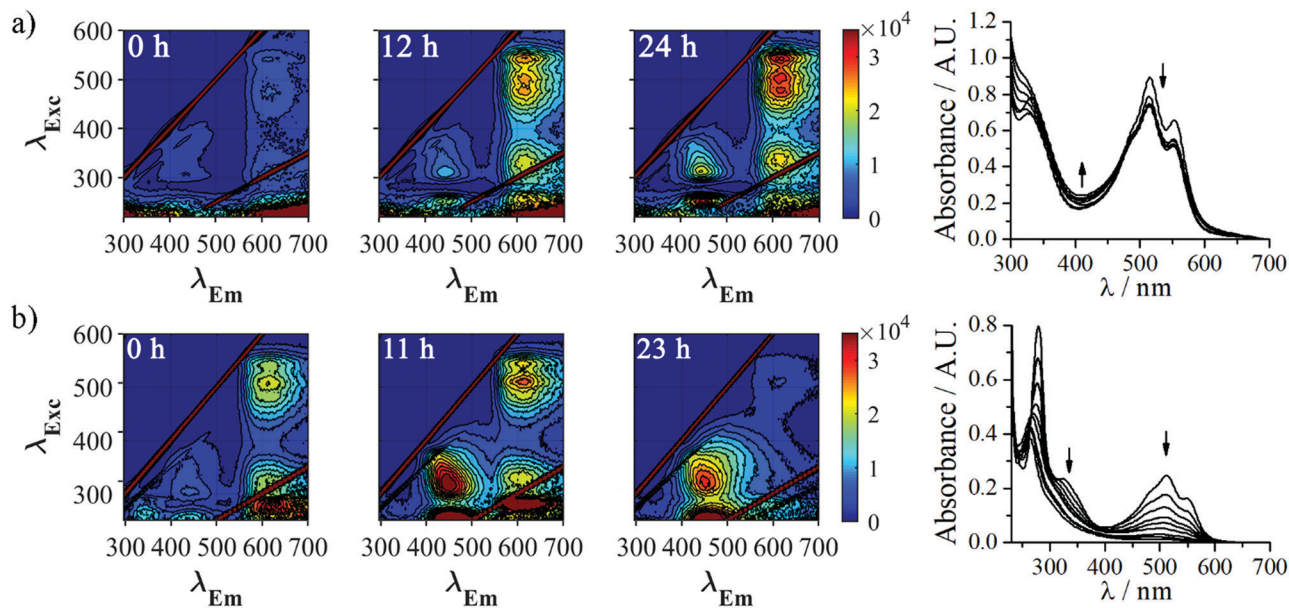*Phys. Chem. Chem. Phys.*, 2020, **22**, 9534–9542 | **9539**

Fig. 6 Evolution of the EEMs (left panel) and UV–vis absorption spectra (right panel) of the lake irradiated aqueous solution: (a) $h\nu$ = 420 nm (total irradiation time = 24 h) and (b) $h\nu$ = 300 nm (total irradiation time = 23 h).

whereas others can be clearly affected by the presence of an aluminium atom coordinated to CA (fluorescence quantum yield of lake was reported to be lower than that of CA).[32] In this regard, the metal can have an impact on the photochemistry of the lake. To further investigate this, air-equilibrated lake aqueous solutions were irradiated using two different lamps. The effect of the excitation wavelength on the spectroscopic profile was studied. Briefly, under both experimental conditions, UV–vis absorption spectra showed a decrease in the total absorbance as the reaction progressed (Fig. 6). This agrees with the net consumption of the reactant as a consequence of induced photodegradation. Fluorescence EEMs show the appearance of, at least, two spots in the Ex/Em domains of 315/455 nm and 485/495 nm (Fig. 6 and Fig. S9 and S10, ESI†). The latter excitation–emission bands are ascribed to the contribution of a carminic-like chromophore (see the normalized emission spectra depicted in Fig. S11a, ESI†).

As it was described for CA, the photodegradation pattern of lake showed spectroscopic differences when comparing between the two excitation wavelengths used. This is more evident when the normalized difference (ND) spectra shown in Fig. S8 (ESI†) are inspected. This fact is indicative of the formation of distinctive photoproducts when the lake is subject to a different source of irradiation. Interestingly, the excitation and emission spectroscopic patterns of the latter photoproducts are the same as those obtained from a CA irradiated solution (Fig. S11c and d, ESI†). Therefore, it can be concluded that both pigments give rise to the formation of similar photoproducts.

At the initial steps of the photochemical reaction of the lake, EEMs showed a particular trend. Briefly, a clear increase in the fluorescence intensity of the excitation–emission bands ascribed to the carminic chromophore in the lake, Ex/Em
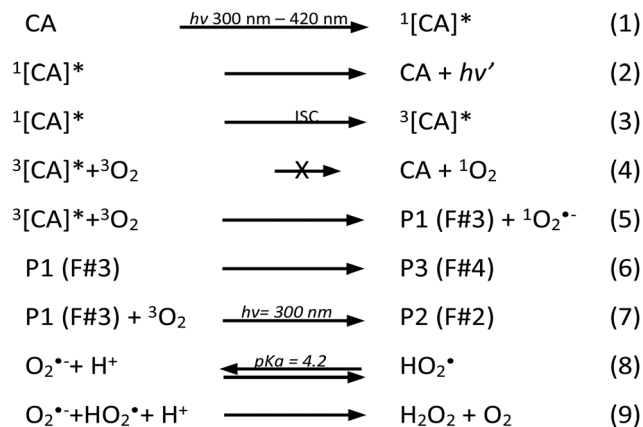
485/495 nm, was observed (Fig. S11b, ESI†). This can be accounted for by assuming the release of a coordinated CA[19] from the photoexcited lake which gives rise to a more fluorescent chromophore that would then follow photodegradation.

4. Conclusions

The quantitative characterization of the non-radiative decay efficiency of photoexcited CA together with lake and related pigments, by laser induced optoacoustic spectroscopy (LIOAS), reveals that for all the investigated compounds, almost all the absorbed energy is released as prompt heat to the media. In addition, these pigments showed extremely low or null capability to produce reactive oxygen species such as hydrogen peroxide (H_2O_2) and singlet oxygen ($^1O_2$). In addition, a comprehensive study of the photochemical degradation of CA and lake, as representative examples, is herein reported. Although with a rather low efficiency, in aqueous media both pigments follow photochemical degradation when subject to elapsed photoexcitation in the UVB, UVA and visible regions. Some relevant aspects of the main mechanism of the reaction were resolved and the spectroscopic features of the photoproducts were identified. Data obtained are summarized in Scheme 2.

On the other hand, the photoexcited lake would first lead to the release of a CA-like chromophore. The latter chromophore would then follow a similar photochemical trend to CA (Scheme 2). Additional experiments are needed to fully address the mechanisms involved in the photochemical degradation of the lake.

The use of non-invasive spectroscopic measurements in combination with chemometric analysis to further address

$$CA \xrightarrow{h\nu\ 300\ nm\ -\ 420\ nm} {}^1[CA]^* \quad (1)$$

$${}^1[CA]^* \longrightarrow CA + h\nu' \quad (2)$$

$${}^1[CA]^* \xrightarrow{ISC} {}^3[CA]^* \quad (3)$$

$${}^3[CA]^* + {}^3O_2 \xrightarrow{\ \ X\ \ } CA + {}^1O_2 \quad (4)$$

$${}^3[CA]^* + {}^3O_2 \longrightarrow P1\ (F\#3) + {}^1O_2^{\bullet-} \quad (5)$$

$$P1\ (F\#3) \longrightarrow P3\ (F\#4) \quad (6)$$

$$P1\ (F\#3) + {}^3O_2 \xrightarrow{h\nu=\ 300\ nm} P2\ (F\#2) \quad (7)$$

$$O_2^{\bullet-} + H^+ \xleftarrow{pKa\ =\ 4.2} HO_2^{\bullet} \quad (8)$$

$$O_2^{\bullet-} + HO_2^{\bullet} + H^+ \longrightarrow H_2O_2 + O_2 \quad (9)$$

Scheme 2 Suggested general mechanism for CA photodegradation.

the fingerprint of photoinduced aging of these widely used pigments may have several ramifications; in particular, in art conservation and restoration, and in food analysis.

Conflicts of interest

There are no conflicts of interest to declare.

Acknowledgements

References

1 R. L. Feller, *Artists' Pigments: Volume 1: A Handbook of their History and Characteristics*, Cambridge, 1987.

2 J. Müller-Maatsch and C. Gras, *The 'Carmine Problem' and Potential Alternatives*, Elsevier Ltd, 2016, vol. 80.

3 A. Claro, M. J. Melo, J. S. Seixas de Melo, K. J. van den Berg, A. Burnstock, M. Montague and R. Newman, Identification of red colorants in van Gogh paintings and ancient Andean textiles by microspectrofluorimetry, *J. Cult. Herit.*, 2010, **11**, 27–34.

4 A. Seldes, J. E. Burucúa, G. Siracusano, M. S. Maier and G. E. Abad, Green, yellow, and red pigments in South American painting, 1610-1780, *J. Am. Inst. Conserv.*, 2002, **41**, 225–242.

5 E. P. Tomasini, F. Marte, V. P. Careaga, C. R. Landa, G. Siracusano and M. S. Maier, Virtuous colours for Mary. Identification of lapis lazuli, smalt and cochineal in the Andean colonial image of Our Lady of Copacabana (Bolivia), *Philos. Trans. R. Soc., A*, 2016, **374**, 2082–2092.

6 P. Biocca, P. Santopadre, G. Sidoti, G. Sotgiu, F. de Notaristefani and L. Tortora, ToF-SIMS study of gilding technique in the fresco Vela della Castità by Giotto's school, *Surf. Interface Anal.*, 2016, **48**, 404–408.

7 E. Phipps, *Cochineal red: the art history of a color*, Metropolitan Museum of Art, New York, 2010.

8 A. Serrano, M. M. Sousa, J. Hallett, J. A. Lopes and M. C. Oliveira, Analysis of natural red dyes (cochineal) in textiles of historical importance using HPLC and multivariate data analysis, *Anal. Bioanal. Chem.*, 2011, **401**, 735–743.

9 M. S. Maier, S. D. Parera and A. M. Seldes, Matrix-assisted laser desorption and electrospray ionization mass spectrometry of carminic acid isolated from cochineal, *Int. J. Mass Spectrom.*, 2004, **232**, 225–229.

10 A. Amat, C. Clementi, C. Miliani, A. Romani, A. Sgamellotti and S. Fantacci, Complexation of apigenin and luteolin in weld lake: A DFT/TDDFT investigation, *Phys. Chem. Chem. Phys.*, 2010, **12**, 6672–6684.

11 L. Carta, M. Biczysko, J. Bloino, D. Licari and V. Barone, Environmental and complexation effects on the structures and spectroscopic signatures of organic pigments relevant for cultural heritage: the case of Alizarin and Alizarin-Mg(ɪɪ)/Al(ɪɪɪ), *Phys. Chem. Chem. Phys.*, 2014, **16**, 2897–2911.

12 A. Amat, C. Miliani, A. Romani and S. Fantacci, DFT/TDDFT investigation on the UV-vis absorption and fluorescence properties of alizarin dye, *Phys. Chem. Chem. Phys.*, 2015, **9**, 6374–6382.

13 J. A. Fernández-López, J. M. Angosto, P. J. Giménez and G. León, Thermal Stability of Selected Natural Red Extracts Used as Food Colorants, *Plant Foods Hum. Nutr.*, 2013, **68**, 11–17.

14 G. Favaro, C. Miliani, A. Romani and M. Vagnini, Role of protolytic interactions in photo-aging processes of carminic acid and carminic lake in solution and painted layers, *J. Chem. Soc., Perkin Trans. 2*, 2002, 192–197.

15 J. S. Arney, A. J. Jacobs and R. Newman, The Influence of Oxygen on the Fading of Organic Colorants, *J. Am. Inst. Conserv.*, 1979, **18**, 108–117.

16 V. L. Beltran, J. Druzik and S. Maekawa, Large-scale assessment of light-induced color change in air and anoxic environments, *Stud. Conserv.*, 2012, **57**, 42–57.

17 A. Lerwill, J. H. Townsend, J. Thomas, S. Hackney, C. Caspers and H. Liang, Photochemical colour change for traditional watercolour pigments in low oxygen levels, *Stud. Conserv.*, 2015, **60**, 15–32.

18 B. H. Berrie and Y. Strumfels, Change is permanent: thoughts on the fading of cochineal-based watercolor pigments, *Heritage Sci.*, 2017, **5**, 30.

19 L. M. R. Bowers and S. J. S. Sobeck, Impact of medium and ambient environment on the photodegradation of carmine in solution and paints, *Dyes Pigm.*, 2016, **127**, 18–24.

20 C. Marti, O. Jurgens, O. Cuenca, M. Casals and S. Nonell, Aromatic ketones as standards for singlet molecular oxygen O2 (1Dg) photosensitization. Time-resolved photoacoustic

This journal is © the Owner Societies 2020

Phys. Chem. Chem. Phys., 2020, **22**, 9534–9542 | **9541**

and near-IR emission studies, *J. Photochem. Photobiol., A*, 1996, **97**, 9–16.

21 P. Murasecco-Suardi, E. Gassmann, A. M. Braun and E. Oliveros, Determination of the Quantum Yield of Intersystem Crossing of Rose Bengal, *Helv. Chim. Acta*, 1987, **70**, 1760–1773.

22 F. Ragone, H. H. M. Saavedra, P. M. D. Gara, G. T. Ruiz and E. Wolcan, Photosensitized Generation of Singlet Oxygen from Re(ı) Complexes: A Photophysical Study Using LIOAS and Luminescence Techniques, *J. Phys. Chem. A*, 2013, **117**, 4428–4435.

23 S. E. Braslavsky and G. E. Heibel, Time-Resolved Photothermal and Photoacoustic Methods Applied to Photoinduced Processes in Solution, *Chem. Rev.*, 1992, **92**, 1381–1410.

24 H. H. Martinez Saavedra, F. Ragone, C. A. Franca, G. T. Ruiz, P. M. D. Gara and E. Wolcan, Solvent effects on the photophysical properties of Bu4N[(4,4′-bpy)Re(CO)$_3$(bpy-5,5′-diCOO)] complex. A combined experimental and computational study, *J. Organomet. Chem.*, 2016, **817**, 26–35.

25 H. Stapeifeidt, H. Jun and L. H. Skibstedt, Fluorescence properties of carminic acid in relation to aggregation, complex foration and oxygen activation in aqueous food models, *Food Chem.*, 1993, **48**, 1–11.

26 M. M. Gonzalez, M. L. Salum, Y. Gholipour, F. M. Cabrerizo and R. Erra-Balsells, Photochemistry of norharmane in aqueous solution, *Photochem. Photobiol. Sci.*, 2009, **8**, 1139–1149.

27 M. M. Gonzalez, J. Arnbjerg, M. P. Denofrio, R. Erra-balsells, P. R. Ogilby and F. M. Cabrerizo, One- and Two-Photon Excitation of -Carbolines in Aqueous Solution: pH-Dependent Spectroscopy, *Photochem. Photophys.*, 2009, 6648–6656.

28 F. A. O. Rasse-Suriani, M. Paula Denofrio, J. G. Yañuk, M. Micaela Gonzalez, E. Wolcan, M. Seifermann, R. Erra-Balsells and F. M. Cabrerizo, Chemical and photochemical properties of chloroharmine derivatives in aqueous solutions, *Phys. Chem. Chem. Phys.*, 2016, **18**, 886–900.

29 F. M. Cabrerizo, M. L. Dantola, A. H. Thomas, C. Lorente, A. M. Braun, E. Oliveros and A. L. Capparelli, Photooxidation of pterin in aqueous solutions: Biological and biomedical implications, *Chem. Biodiversity*, 2004, **1**, 1800–1811.

30 F. A. O. Rasse-Suriani, F. S. García-Einschlag, M. Rafti, T. Schmidt De León, P. M. David Gara, R. Erra-Balsells and F. M. Cabrerizo, Photophysical and Photochemical Properties of Naturally Occurring normelinonine F and Melinonine F Alkaloids and Structurally Related N(2)- and/or N(9)-methyl-β-carboline Derivatives, *Photochem. Photobiol.*, 2018, **94**(1), 36–51.

31 H. Kunkely and A. Vogler, Absorption and luminescence spectra of cochineal, *Inorg. Chem. Commun.*, 2011, **14**, 1153–1155.

32 K. Jørgensen and L. H. Skibsted, Light sensitivity of cochineal. Quantum yields for photodegradation of carminic acid and conjugate bases in aqueous solution, *Food Chem.*, 1991, **40**, 25–34.

33 L. Jespersen, L. D. Stramdahl, K. Olsen and L. H. Skibsted, Heat and light stability of three natural blue colorants for use in confectionery and beverages, *Eur. Food Res. Technol.*, 2005, **220**, 261–266.

34 C. Miliani, A. Romani and G. Favaro, A spectrophotometric and fluorimetric study of some anthraquinoid and indigoid colorants used in artistic paintings, *Spectrochim. Acta, Part A*, 1998, **54**, 581–588.

35 T. Gensch and C. Viappiani, Time-resolved photothermal methods: accessing time-resolved thermodynamics of photoinduced processes in chemistry and biology, *Photochem. Photobiol. Sci.*, 2003, **2**, 699–721.

36 Y. Tang and G. J. Smith, Fluorescence and photodegradation of Xuan paper: The photostability of traditional Chinese handmade paper, *J. Cult. Herit.*, 2013, **14**, 464–470.

37 M. J. Melo, L. J. Ferreira, J. A. Parola and J. S. Seixas de Melo, *Appl. Photochem.*, 2016, **92**, 499–530.

9542 | *Phys. Chem. Chem. Phys.*, 2020, **22**, 9534–9542

This journal is © the Owner Societies 2020